SolarPACES 2023, 29th International Conference on Concentrating Solar Power, Thermal, and Chemical Energy Systems

Solar Collector Systems

https://doi.org/10.52825/solarpaces.v2i.758

Published: 28 Aug. 2024

Characterization of an Induction Heating System Used as a Solar Simulator

Analysis of Thermal Performance, Experimental Challenges, and Enhancements

Rand Hasan Khrishi[1,*], Marta Laporte-Azcué[1], and María de los Reyes Rodriguez-Sanchez[1]

[1] Universidad Carlos III de Madrid, Spain

*Correspondence: Rand Hasan Khrishi, 100479201@alumnos.uc3m.es

Abstract. This report delves into the thermal behaviour of solar receiver tubes under induction heating, a key component in concentrated solar power (CSP) technology. Experimental investigations were conducted to understand the temperature distribution and challenges associated with induction heating. A stainless-steel tube was heated using an inductor and subjected to airflow. Initial tests revealed temperature deviations caused by the electromagnetic field and thermocouple interference. Adjustments were made in subsequent trials, including thermocouple repositioning, extended heating times, and consistent camera calibration. Additional experiments explored the effects of inserting iron plates in between the tube and the inductor coil. Results showcased varying temperature profiles for different configurations. In all the cases analysed, there is penetration of the magnetic field within the thickness of the tube walls, simplified as volumetric heat generation. Overall, these findings enhance our comprehension of induction heating dynamics to test CSP components in a small-laboratory scale that would potentially offer insights for system optimization.

Keywords: Concentrated Solar Power, Solar Receiver Tubes, Induction Heating.

1. Introduction

In recent years, the utilization of concentrated solar power (CSP) technology has gained significant popularity due to its potential for providing a reliable and renewable source of energy. The CSP tower systems use mirrors or lenses to concentrate sunlight onto a receiver located at the top of a tower. The concentrated solar energy is absorbed by the receiver, which converts it into thermal energy, ultimately generating electricity [1]. To ensure the efficient and reliable operation of the solar receiver, which is a key element of these plants and one of their most critical subsystems [2], it is crucial to understand its thermomechanical behavior under varying operating conditions. For this purpose, experimental tests are necessary, particularly when dealing with new materials and designs. In small-scale testing facilities, induction heating is often used to simulate heating conditions in concentrated solar power plant receiver tubes. However, it has been noted

that induction heating can penetrate stainless-steel pipes, resulting in volumetric generation, which affects the temperature along the tube wall [3]. Therefore, experimental tests are suggested to investigate this phenomenon for implementing induction heating in laboratory tests involving closed loops.

2. Experimental setup

The subsequent experimental facility was designed to analyze variations in temperature profiles along the receiving tube. In the context of this study, the receiving tube is a stainless-steel pipe with a diameter of 19.05 mm and a thickness of 1.65 mm. An airflow of 800 l/min was directed through the tube's interior, which was subsequently heated to elevated temperatures using an inductor coil positioned 3 mm away from the tube's facing surface, as illustrated in Figure 1 a). The power supplied by the heater is set to 1 kW and remains constant in all the experiments conducted to ensure consistent and controlled heating condition.

The goal of this job is to characterize the heating process of an induction heater to be used as a solar simulator for concentrating solar power (CSP) systems. With this system, we can achieve fluxes of 1 MW/m², similar to those in solar power towers. The shape of the coil allows for circumferential variations in temperature, similar to those in tubular central receivers, and it is possible to use molten salts as the heat transfer fluid (HTF). However, for characterization purposes and to measure the circumferential and radial temperature profiles accurately, the mass flow rate must be air (a fluid that can be released into the environment). The 1 kW power represents 10% of the total nominal power of the inductor. This lower power setting is used to prevent damage to the tube and to avoid exceeding the temperature limit of the infrared camera.

The comprehensive induction heating system comprised a water tank, water pump, refrigeration unit, and the EFD Sinac 6SH 350 kHz inductor heater by EFD INDUCTION. The latter encompasses a frequency converter, a heating station, and an induction coil. The coil is configured as a square prism with dimensions of 100 mm in length, 7 mm in width, and 10 mm in thickness. This prism is enveloped by a magnetic composite flux concentrator measuring 4 mm in thickness. Notably, the cited induction system has been previously utilized in [4]-[6] for analogous purposes. The experimental facility was monitored using two infrared cameras (Optris PI640 15x11), one facing the lateral side of the tube as shown in Figure 1 b), and the other located below the tube, as seen in Figure 1 c). It is worth mentioning that the tube was left open to facilitate the recording of heating effects and behavior using the bottom camera.

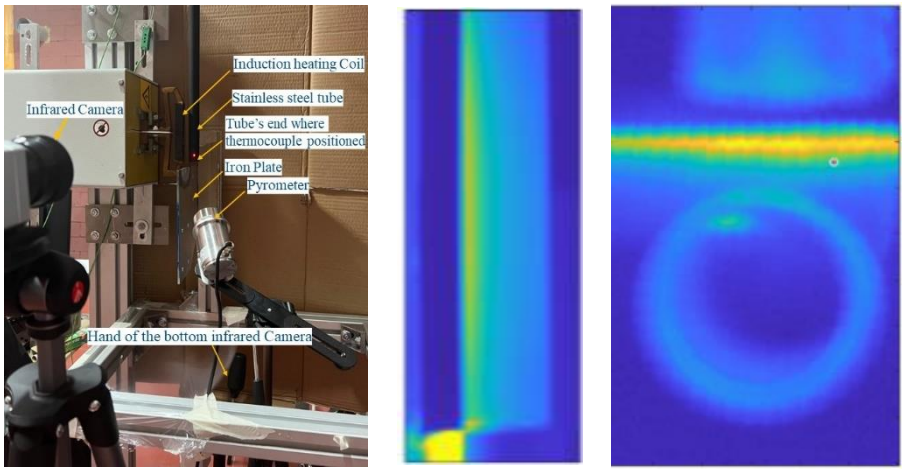

a b c

Figure 1. *a) Experimental facility, b) lateral camera view, c) bottom camera view.*

However, since the tube is left open, the magnetic field lines may circulate around it, which may lead to unexpectedly high temperatures at the tube rear-side, deviating from that in solar central receiver tubes. Hence, to prevent this, an iron plate was inserted between the inductor and the tube near the end edge of the tube, and the subsequent results were compared. Additionally, two encapsulated thermocouples type T were carefully positioned inside at the inlet and at the end of the tube to monitor the inlet and outlet temperature of the airflow during the experiment, and a CTlaser LTCF2 pyrometer was located at the lateral side of the tube to monitor the appropriate behavior of the lateral camera.

3. Experimental procedure

3.1 First step results and initial challenges

The analysis of the preliminary experimental recordings from both cameras yielded temperature distribution graphs at various angles of the stainless-steel tube. Figure 2) presents the outcomes of this stage, including the temperature distribution captured using both cameras at the main angles of the tube as clarified in figure 2 a). Figure 2 b) and 2 c) show the results corresponding to the bottom camera for the outer and inner tube wall, respectively, and Figure 2 d) shows the lateral camera temperatures recorded for the outer tube wall. However, this phase encountered certain challenges that warrant discussion.

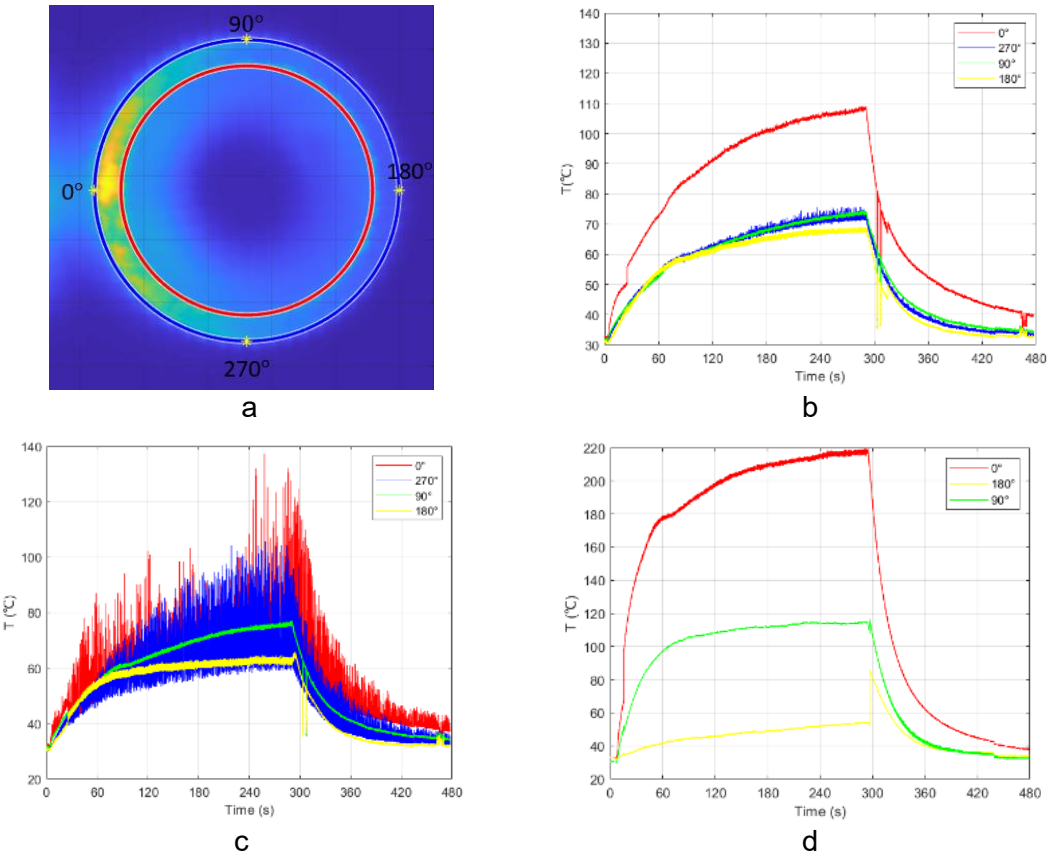

Figure 2. *One plate case first experiment results: a) tube angles, b) bottom camera results at the outer tube wall, b) bottom camera results at the inner tube wall, and c) lateral camera results.*

One significant challenge was encountered due to the presence of the lower thermocouple inside the tube, leading to substantial noise in the temperature readings, as shown in Figure 2 b), where the temperature distribution of the inner radius of the tube is depicted. To address this issue, adjustments were made by slightly repositioning the thermocouples from the bottom, resulting in noise reduction. Another difficulty was faced during the analysis, involving the identification of the steady-state period based on the graphs obtained it is observed that a 4-minute heating was insufficient to reach a steady state. This led to the requirement of an extended duration for the heating to ensure more comprehensive data collection. Furthermore, an undesirably large discrepancy in the tube temperatures, as recorded by the lateral and bottom cameras, was observed, which was attributed to differences in the cameras' field of view. Despite these initial challenges, the initial analysis yielded valuable insights. In response, several measures were implemented to enhance the accuracy and reliability of the data. Subsequent experiments were conducted to address these issues and achieve improved analytical results.

3.2 Improved solutions

In response to the challenges encountered during the initial experiment, a subsequent trial was meticulously carried out under the same conditions but including several adjustments. First, the lower thermocouple, the one measuring the airflow outlet temperature, was slightly pulled up to reduce noise interference and significantly improve temperature measurement accuracy along the inner wall of the tube. Secondly, the duration of the heating process was extended to 5 minutes, ensuring the system reached a steady-state condition, enabling more reliable analysis

of temperature profiles, heat flux, and heat generation within the tube at that stage. Lastly, special attention was given to achieve consistent backgrounds for both cameras, minimizing variations in temperature readings to more acceptable ones. The calibration process effectively resolved the observed discrepancy in the outer tube temperatures recorded by the lateral and bottom cameras.

3.3 Further investigations

To expand the study, two additional experimental cases were executed: one without inserting any iron plate between the inductor and the tube and the other with two plates inserted symmetrically around the tube, see Figure 3. For the latter configuration, one iron plate was positioned between the tube and the inductor, mirroring the setup employed in previous experiments. Concurrently, a second iron plate was symmetrically inserted on the opposite side of the tube, effectively sandwiching the tube outlet between the two plates. The results of these cases were compared to the initial experiment with a single plate to assess their impact on temperature distribution.

a b

Figure 3. *a) No plate experiment setup, and b) two plates experiment setup.*

4. Results and discussion

Figure 4 visually presents refined experiment results using a single iron plate setup, depicting sequential temperature changes over time at different angles of the stainless-steel tube. Figure 4 a) displays outer wall outcomes from the bottom camera view, while Figure 4 b) presents corresponding inner wall results. Additionally, Figure 4 c) showcases temperature data from the lateral camera. The enhancements discussed in section 3.2 effectively addressed challenges from the initial experiment earlier shown in Figure 2, improving data accuracy and reliability. Although inner wall temperature noise is notably reduced, some interference remains due to the thermocouple. Further adjusting the bottom thermocouple position was rejected to ensure accurate airflow temperature measurements.

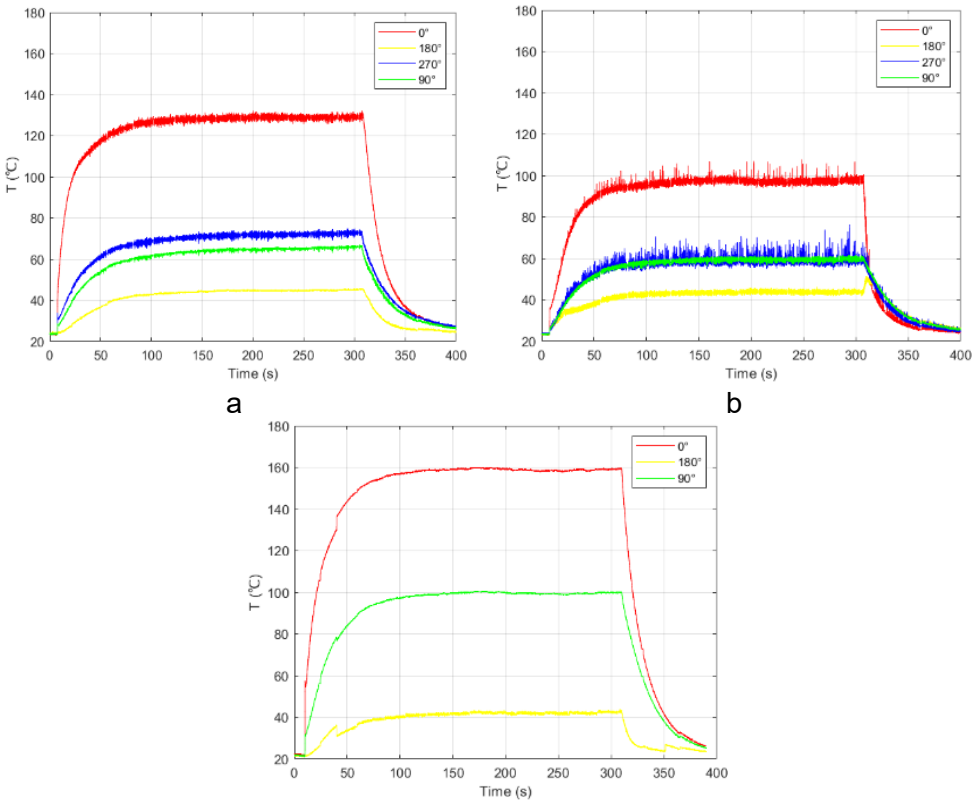

Figure 4. *One plate case refined experiment results: a) outer wall temperature variation, b) inner wall temperature variation, and c) lateral view temperature variation.*

The two additional experiments, without plates and with two plates, revealed significant differences in temperature and noise. It is worth to mention that the noise at the no plate case is more significant than that in the other two cases (with one plate, or two plates). Figure 5 depicts results without inserted plates, while Figure 6 exhibits the outcomes with two plates. Moreover, it is important to note that the case without iron plates resulted in notably higher temperature increases at the outer tube wall compared to configurations with one or two iron plates.

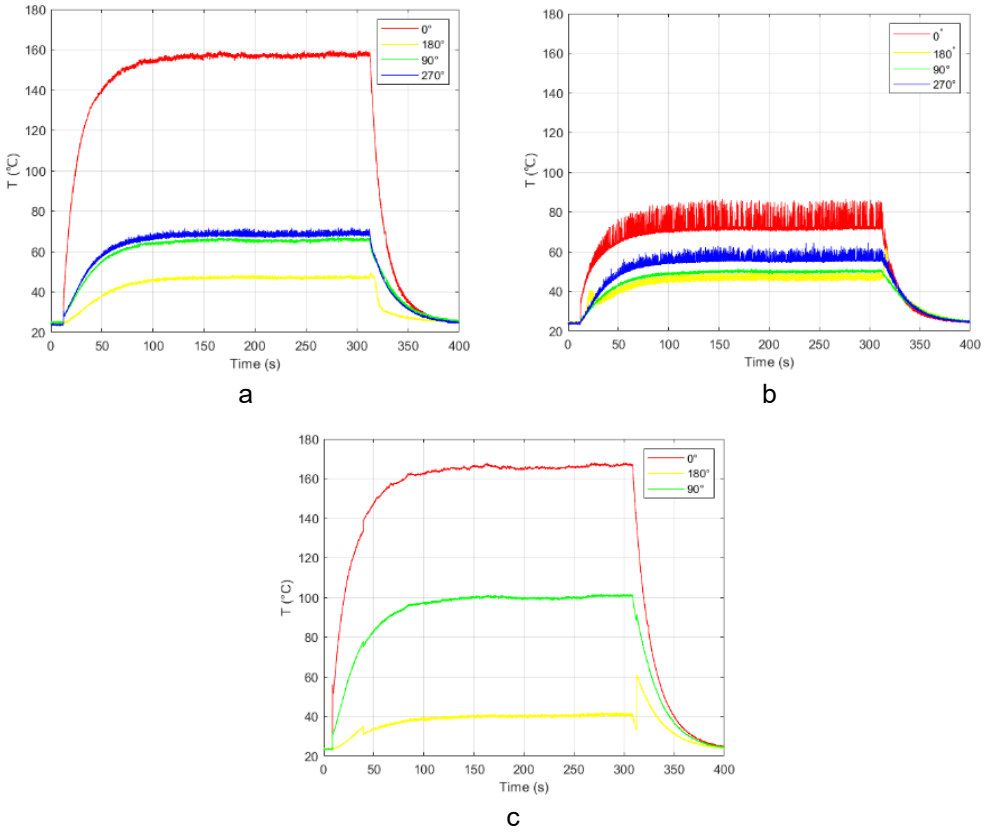

Figure 5. *No plate case results: a) outer wall temperature variation, b) inner wall temperature variation, c) lateral view temperature variation.*

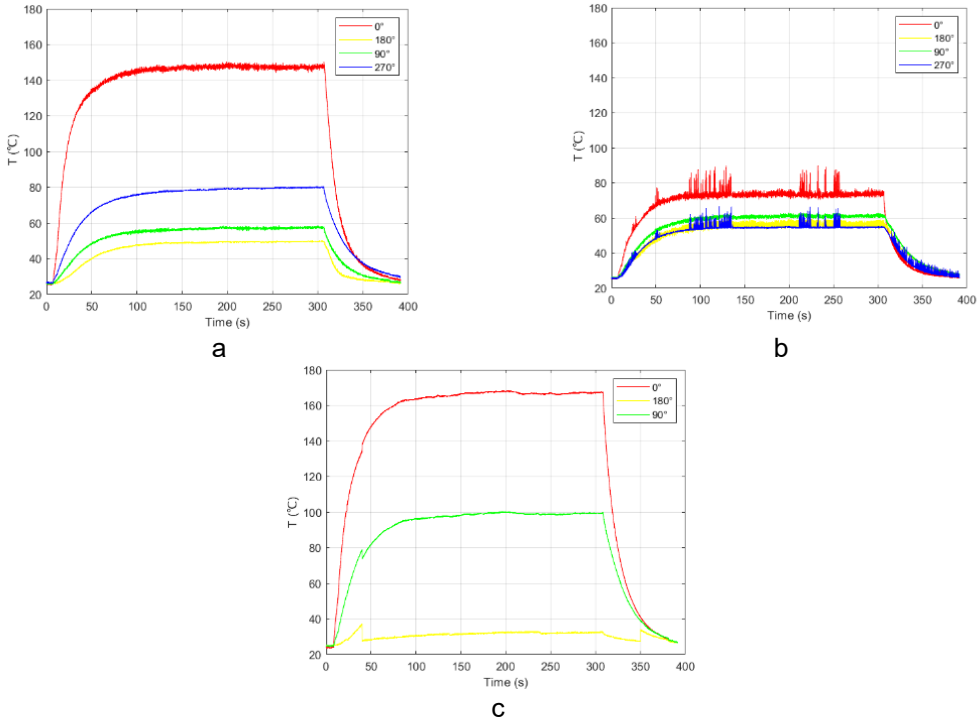

Figure 6. *Two plates case results: a) outer wall temperature variation, b) inner wall temperature variation, c) lateral view temperature variation.*

In the two plates experiments, it is observed that the interaction between the inductor's magnetic field and iron plates' causes the thermocouple inside the tube to temporarily remain centered in the tube cross section, keeping them away from the inner wall. This leads to reduced noise during experiments, less consistently noticeable throughout the process at the inner wall of the tube. The consistency of temperature readings across all cases (no plate, one plate, and two plates) that was observed in the lateral camera recordings is attributed to the camera's focused view exclusively on the tube, excluding the plates. In contrast, the bottom camera's field of view, influenced by the presence of plates, led to temperature variations. This was most evident in the no plate scenario, where both cameras yielded nearly identical temperatures.

The investigation into solar receiver tube behavior under induction heating has unveiled intricate temperature distribution patterns influenced by the interplay of induction heating, volumetric heat generation, and iron plate positioning near the lower edge of the tube. Additional results are visually represented in Figure 7, showing angular temperature distribution for outer and inner tube walls in Figures 7 a) and 7 b), respectively, and radial temperature distribution from inner to outer wall in Figure 7 c).

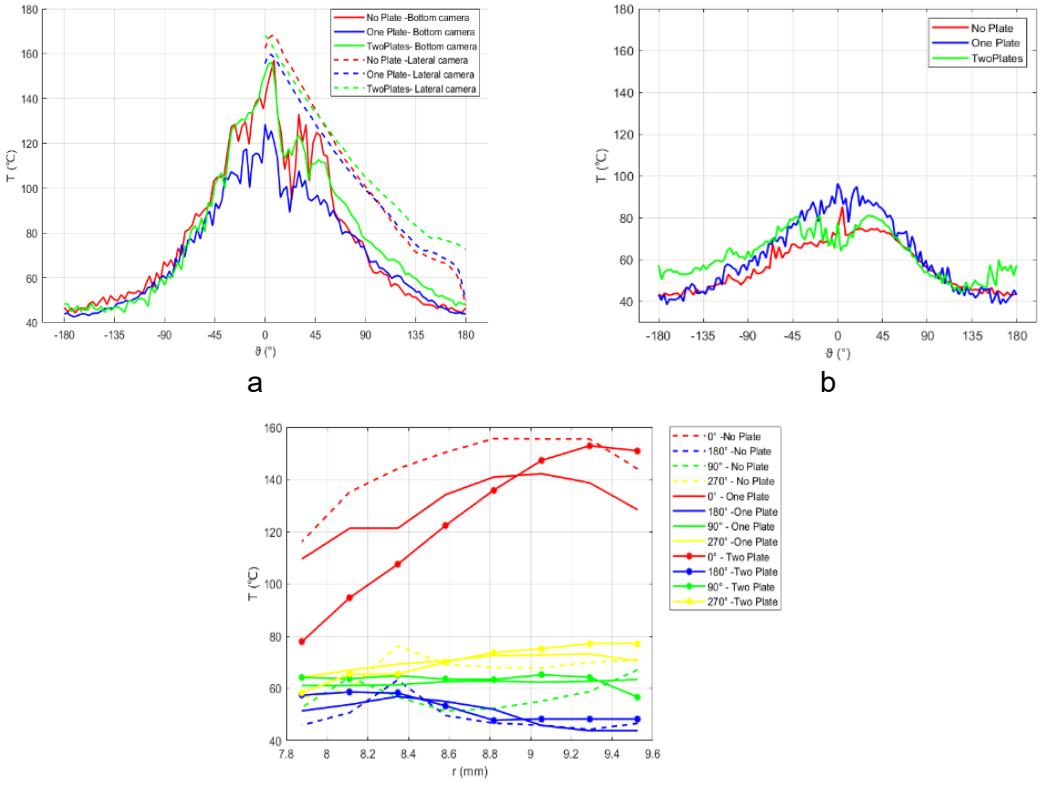

Figure 7. *Angular and radial temperature distributions. a) angular distribution - outer wall, b) angular temperature - inner wall, c) radial temperature distribution - inner to outer wall transition.*

Analyzing angular temperature distribution, Figures 7a) and 7b) reveal iron plates' significant impact on heat dispersion. Looking at the bottom camera recordings, the outer wall temperature distribution is quite similar for the three cases at the rear portion of the tube, from 60º to 180º. However, at the front, the one plate case diverges from the other two, showing lower temperatures. On the other hand, the lateral camera results show a similar trend in qualitative terms, yet greater temperatures are observed, as previously mentioned. Regarding the inner wall

temperature, the no plate case is in between the other two, matching the one plate scenario results near the back of the tube and the two plates experiments results at the front.

As for the temperature differences between the inner and outer tube wall temperatures, the three scenarios show a similar outcome, with nearly-negligible gradients at the rear-side. Hence, the electromagnetic field lines do not seem to surround the tube at the bottom edge, or at least have a significant effect, in this specific setup (power, coil-to-tube distance, etc.). This observation is particularly relevant in the no plates experiments. The scenario with the most significant gradient from inner to outer tube wall at the tube's rear side is the two plates case, suggesting an interaction between the plates, heated by the inductor, and the tube's bottom rim. At the tube's front (0º-outer tube wall), the one plate scenario has the lowest differences between inner and outer tube wall temperatures, likely due to radiation heat from the heated plate. Overall, since the electromagnetic field appears to have little impact on the tube's rear side, the configuration without plates may suffice for analyzing volumetric heat generation in the tube.

On the other hand, when examining the complete radial temperature distribution from the inner to the outer radius, as shown in Figure 7 c), the volumetric heat generation can be observed at the tube front: the three cases present their maximum temperature within the tube walls, rather than at the outer tube wall. The no plate case displays higher maximum temperature inside the tube wall, followed by the two plates scenario. Still, the greater temperature gradient between the tube outer wall temperature and the maximum within the wall occurs at the one plate case, which once more may be related to the radiation heat of the iron plate incident on the tube edge.

Among the three experimental setups, the only significant change observed was in the temperature of the tube, particularly at the front side near the inductor. Initially, it was assumed that without the iron plate, the magnetic field would cause the far side of the tube to reach temperatures similar to those near the inductor. This hypothesis was tested through experiments. When the iron plate was absent, significant temperature variations around the tube were observed. With the iron plate in place, the temperature variations around the tube remained similar to those observed without the plate. Further investigation involved the addition of two iron plates with the tube positioned between them, which resulted in similar outcomes to the single-plate configuration, though with different temperature values.

5. Conclusions

In this study, the thermal behavior of solar receiver tubes under induction heating, an essential element of concentrated solar power (CSP) technology, was explored. Through a series of experimental investigations, insights into temperature distribution and challenges associated with induction heating were gained. Deviations in temperature caused by electromagnetic field effects and thermocouple interference were revealed in the initial tests. To address these challenges, the experimental approach was refined, including thermocouple repositioning, extension of heating times, and consistent camera calibration. In further experiments, various plate configurations were tested around the tube, including no plates and two plates sandwiching it, in comparison to using a single plate. Despite producing different temperature profiles, none of these plate configurations succeeded in reducing heat generation at the tube's front. Additionally, temperature distribution at the tube's rear in all three cases suggested that electromagnetic field lines might not be strong enough to affect temperatures in that region. Therefore, no plates were necessary to shield the tube from this effect, which was supported by consistent temperature readings for both cameras at the outer diameter at 180º when plates were absent. The results emphasize the importance of considering heat generation in analytical models based on data from induction heating experiments conducted in such facilities.

Overall, these findings notably improve the understanding of induction heating dynamics for testing CSP components at a small laboratory scale. By the unraveling of the complexities of induction heating, iron plate effects, and resulting temperature distributions, valuable insights are offered for the optimization of solar power systems. The present work constitutes the starting point to further investigate induction heating in tubes, having successfully designed an experimental facility and developed a methodology for that end. Future steps involve the investigation of the volumetric heat generation for different operation conditions, such as inductor power, coil-to-tube distance, and air flow. A wider array of cases may aid the understanding of the most relevant parameters leading to that phenomenon. Moreover, the heating efficiency of the system is yet to be addressed.

Data availability statement

The data supporting the results in this article are available upon request from the corresponding author. Due to legal, and third-party restrictions, full public deposition is not currently feasible. We aim to facilitate data access while respecting these considerations. For inquiries, please contact the corresponding author. Future efforts may explore depositing data in a suitable public repository to enhance accessibility and reproducibility.

Acknowledgments:

The authors gratefully acknowledge the financial support provided by the Grant PID2021-122895OB-I00 funded by MCIN/AEI/10.13039/501100011033 and by "ERDF A way of making Europe", the Grant TED2021-129326B-I00 funded by MCIN/AEI/10.13039/501100011033 and by "European Union NextGenerationEU/PRTR", and the Grant "Beca Leonardo a Investigadores y Creadores Culturales 2022 de la Fundación BBVA". And would like to express heartfelt appreciation to all individuals and organizations who contributed to the successful completion of this research.

Author contributions:

- Rand Khrishi: Conceptualization, Methodology, Experimental Work, Data Analysis, Writing - Original Draft, Review, and Editing.
- Marta Laporte-Azcué: Conceptualization, Methodology, Writing - Review and Editing, Supervision, Review, and Audit.
- Maria de Los Reyes Rodriguez-Sanchez: Conceptualization, Writing - Review and Editing, General Supervision, Final Audit.

Competing Interests:

The authors declare no competing interests.

References

[1] International Renewable Energy Agency (IRENA), "Renewable energy technologies cost analysis series Concentrating Solar Power, Vol 1: Power Sector Issue 2/5, June, 2012, https://www.irena.org/Publications (accessed Augst 15, 2023)

[2] M. Mehos, H. Price, R. Cable, D. Kearney, B. Kelly, G. Kolb, F. Morse, "Concentrating Solar Power Best Practices Study," NREL, June, 2020, www.nrel.gov/publications (accessed Augst 22, 2024).

[3] E. Cano-Pleite, M. Fernández-Torrijos, D. Santana, and A. Acosta-Iborra, “Heat generation depth and temperature distribution in solar receiver tubes subjected to induction,” Appl. Thermal Eng., vol. 204, Mar. 2022, doi: 10.1016/j.applthermaleng.2021.117902.

[4] M. Fernández-Torrijos, C. Sobrino, J. A. Almendros-Ibáñez, C. Marugán-Cruz, and D. Santana, “Inverse heat problem of determining unknown surface heat flux in a molten salt loop,” International Journal of Heat and Mass Transfer, vol. 139, pp. 503–516, Aug. 2019, doi: 10.1016/j.ijheatmasstransfer.2019.05.002.

[5] M. Fernández-Torrijos, C. Sobrino, C. Marugán-Cruz, and D. Santana, “Experimental and numerical study of the heat transfer process during the startup of molten salt tower receivers,” Appl. Thermal Eng. vol. 178, September, 2020, doi: 10.1016/j.applthermaleng.2020.115528.

[6] M. R. Rodríguez-Sánchez, A. Pueyo-Balsells, A. Montoya, and J. A. Artero-Guerrero, “Solar simulator based on induction heating to characterize experimentally tubular solar central receivers,” Appl. Thermal Eng. vol.220, Feb, 2023, doi:10.1016/j.applthermaleng.2022.119781.